THE JOURNAL OF PHYSICAL CHEMISTRY B



Article

# Temperature of Peptide Ions Generated by Matrix-Assisted Laser Desorption Ionization and Their Dissociation Kinetic Parameters

Jeong Hee Moon, So Hee Yoon, and Myung Soo Kim

*J. Phys. Chem. B*, **2009**, 113 (7), 2071-2076• Publication Date (Web): 28 January 2009

# Temperature of Peptide Ions Generated by Matrix-Assisted Laser Desorption Ionization and Their Dissociation Kinetic Parameters

**Jeong Hee Moon,*,† So Hee Yoon,‡ and Myung Soo Kim*,‡**

*Department of Chemistry, Seoul National University, Seoul 151-742, Korea, and Systemic Proteomics Research Center, KRIBB, Daejeon 305-806, Korea*

*Received: November 17, 2008; Revised Manuscript Received: December 26, 2008*

Product ion yields in postsource decay and photodissociation at 193 and 266 nm were measured for some peptide ions without a basic amino acid residue ($[Y_6 + H]^+$, $[F_5 + H]^+$, and $[YPFVEPI + H]^+$) generated by matrix-assisted laser desorption ionization (MALDI). Data indicated statistical nature for the dissociation processes. Assuming that peptide ions formed by MALDI are in thermal equilibrium at temperature $T$ and that their dissociation rate constants are specified by the critical energy ($E_0$) and entropy ($\Delta S^{\ddagger}$), a method based on kinetic analysis was devised to determine these parameters simultaneously. The matrix used was found to affect the effective temperature of peptide ions, 2,5-dihydroxybenzoic acid (400−430 K) < sinapinic acid (440 K) < α-cyano-4-hydroxycinnamic acid (460−510 K), in agreement with previous perceptions. $E_0$ of around 0.6 eV and $\Delta S^{\ddagger}$ of −24 eu were smaller than previous quantum chemical results for small model peptide ions.

## Introduction

Tandem mass spectrometry,[1,2] which studies fragmentation of a precursor ion, is of tremendous current interest because of its utility in peptide and protein sequencing. It is well established that the tandem mass spectral patterns for most of small polyatomic ions can be explained within the framework of the microcanonical transition state theory for unimolecular reaction, vs Rice−Ramsperger−Kassel−Marcus theory[3−5] (RRKM). Here, rapid electronic and vibrational relaxations are assumed to ensure quasi-equilibrium of the internal energy of a precursor ion prior to its dissociation. Knowledge about the vibrational frequencies of the precursor at the equilibrium and transition states is needed to calculate a RRKM rate constant. It is known[4,5] that the rate constants calculated with substantially different sets of frequencies are similar as far as the activation entropy ($\Delta S^{\ddagger}$) is kept the same. Hence, the critical energy ($E_0$) and $\Delta S^{\ddagger}$ are regarded as the two parameters affecting a RRKM rate constant. Cases of nonstatistical dissociation have been rare for small polyatomic ions, most frequent being dissociation in a repulsive electronic state.[6] For ultraviolet photodissociation (PD) of peptide ions, we could eliminate such a possibility on the basis of the observation[7,8] that the product ion species formed were essentially the same regardless of the excited electronic states accessed by photoexcitation. This suggests that RRKM can be a good description for dissociation of peptide ions. In fact, there are many reports in the literature that utilized RRKM to explain tandem mass spectral patterns for peptide ions. This group also made a RRKM-based attempt[8] to qualitatively explain time-resolved PD spectra of peptide ions.

The main difficulty in using the RRKM model for peptide ion dissociation is that $E_0$ and $\Delta S^{\ddagger}$ values are unknown. Experimentally, dissociation of peptide ions at low internal energy generates b and y type ions (see refs 9 and 10 for product ion symbols). For peptide ions without an arginine residue, the same types of product ions also dominate even at higher energy. For small peptide ions such as $[G_3 + H]^+$, Paizs and Suhai[11] and Siu and co-workers[12] identified the reaction paths leading to such product ions through quantum chemical calculations at the density functional theory level. Formations of b and y type ions arising from the cleavage of a particular amide bond were found to share a common reaction path until the last steps, which were not rate-determining. Quantum chemical $E_0$ and $\Delta S^{\ddagger}$ values are available from their results. Experimentally, Futrell and co-workers[13] attempted to determine these values by analyzing time-resolved product ion yields in surface-induced dissociation (SID).[14,15] Unlike in photoexcitation, the amount of energy transfer in ion-surface collision is unknown.

The internal energy ($E$), or its distribution ($P_0(E)$), of a precursor ion at the time of its formation is another factor that affects the rate constant. Accurate measurement of $P_0(E)$ by spectroscopic means would be extremely difficult for protonated peptides formed by techniques such as matrix-assisted laser desorption ionization (MALDI).[16−20] Mowry and Johnston[21] attempted to estimate the internal energies of gas phase *n*-alkylamine neutrals formed by laser-induced desorption from sample-matrix mixture, viz. matrix-assisted laser desorption (MALD), by comparing their photoionization (PI) mass spectral patterns with those in temperature-dependent gas phase PI. Vertes et al.[22] used benzyl-substituted benzylpyridinium ions as thermometer molecules and attempted to estimate the average internal energies of these ions in MALDI plume through kinetic analysis of mass spectral patterns. Under the assumption of thermal equilibrium in the matrix plume, the average internal energy measured in the above works can be related to the effective plume temperature.[20] Even though the knowledge about the effective temperature, which would be affected by MALDI conditions such as the matrix used, is critical for understanding the MALDI process, its current estimates vary over a wide range, from around 400 K to higher than 1000 K.[18−24]

The MALDI plume temperature may not be a good measure for the internal energy of a peptide ion formed by MALDI

* Corresponding authors. E-mail: M.S.K., myungsoo@snu.ac.kr; J.H.M., jhdal@kribb.re.kr.
† KRIBB.
‡ Seoul National University.

10.1021/jp810077e CCC: $40.75 
Published on Web 01/28/2009

because their internal energies would be further altered by gas phase proton transfer reactions occurring in the plume that are thought to be mainly responsible for ion formation.[20,25−27] Absence of information on $P(E)$ or effective temperature ($T$) for peptide ions formed by MALDI is a problem in any kinetic attempt to accurately determine $E_0$ and $\Delta S^{\ddagger}$ in their dissociation. Similarly, any attempt to determine $T$ by a kinetic method would suffer from the absence of knowledge about $E_0$ and $\Delta S^{\ddagger}$. At the current level of knowledge, it is needed to devise a method that treats $E_0$, $\Delta S^{\ddagger}$, and $T$ as parameters and determines them simultaneously. A problem in this regard is the fact that a variety of reaction channels compete in the dissociation of a peptide ion. It has been mentioned that the b−y channels are mainly involved in the dissociation of peptide ions without an arginine residue. Because the characteristics of the b−y reaction paths for the cleavage of different amide bonds would be rather similar,[11,28−30] an averaged treatment of these channels, viz. use of a single set of $E_0$ and $\Delta S^{\ddagger}$, can be an acceptable approximation. In the presence of an arginine residue, another set of reaction channels, viz. homolytic cleavage of $C_{\alpha}$−CO bonds,[8,10] participate. The averaged treatment for the latter channels can be an acceptable approximation also, resulting in an additional set of $E_0$ and $\Delta S^{\ddagger}$. However, approximating the whole situation as a single averaged channel problem will be inappropriate because the characteristics of the two sets of channels [b-y (rearrangement, small $E_0$ and small $\Delta S^{\ddagger}$) and homolytic (simple bond cleavage, large $E_0$ and large $\Delta S^{\ddagger}$) channels] would be substantially different. Handling $T$ and two different sets of $E_0$ and $\Delta S^{\ddagger}$ would be a tremendously difficult problem at an early stage of method development.

In this work, a method based on the kinetic analysis of product ion yields in postsource decay (PSD)[31] and time-resolved photodissociation (PD)[8,32] was devised to determine $E_0$, $\Delta S^{\ddagger}$, and $T$ simultaneously for peptide ions generated by MALDI. The first step of this method was the calculation of the RRKM rate−energy relation, $k(E)$, and the internal energy distribution, $P(E)$, with widely different sets of ($E_0$, $\Delta S^{\ddagger}$, $T$). Using $k(E)$ and $P(E)$ obtained with each set of parameters, product ion yields (and their ratios) were calculated. Then, ($E_0$, $\Delta S^{\ddagger}$, $T$) sets compatible with the experimental results were selected by comparing theoretical and experimental yields. The experimental data obtained with three different MALDI matrices were analyzed and compared to improve the accuracy for parameter determination. The method was applied to some peptide ions without a basic amino acid residue for which the averaged treatment could be an acceptable approximation. Details of the method and the results are presented in this paper.

## Experimental Section

A schematic drawing of the home-built MALDI-tandem TOF mass spectrometer equipped with a PD cell assembly used in this work is shown in Figure 1. Details of the main instrument and its operation were reported previously.[8] A brief description is as follows.

The instrument consists of a MALDI source with delayed extraction (20 kV dc and 1.8 kV ac), a first stage TOF analyzer to time-separate the prompt ions generated by MALDI, an ion gate and a second stage TOF analyzer equipped with a reflectron (25 kV). A 337 nm pulse from a nitrogen laser (MNL205-C, Lasertechnik Berlin, Berlin, Germany) is used for MALDI with its fluence kept at 2 times the threshold value in all the experiments. A deflection system[33] is installed inside the first stage TOF to eliminate PSD product ions generated in this region. A cylindrically focused laser pulse at 266 nm (Surelite

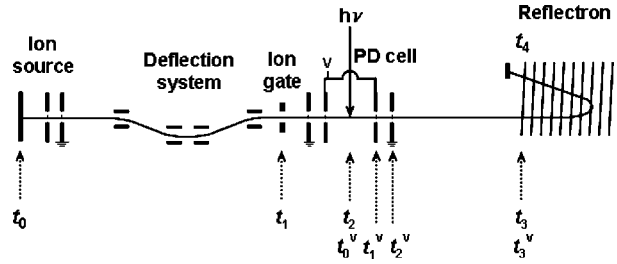


**Figure 1.** Schematic drawing of the MALDI-PD tandem TOF equipped with a PD cell. Relevant time scales for PSD and voltage-on PD are marked. PSD occurs during $t_1$−$t_3$. In-cell and post-cell PDs occur during $t_0^V$−$t_1^V$ and $t_2^V$−$t_3^V$, respectively.

III-10, Continuum, Santa Clara, CA) or at 193 nm (PSX-100, MPB Communication Inc., Montreal, Quebec) is irradiated at the first time focus in synchronization with the lowest $m/z$ isotopomer of a peptide ion. To minimize multiphoton effect, PD laser intensity is reduced until intensity-dependent change in spectral pattern is not observed. The output from the MCP detector is digitized, thresholded, Gaussian-fitted, and averaged.[34] Finally, the laser-off spectrum (PSD) is subtracted from the laser-on spectrum to obtain the laser-induced change or the PD spectrum.

Use of the voltage-floated PD cell for time-resolved study was reported previously.[8,32] The PD cell consists of four grid electrodes (E1−E4). E1 and E4 are grounded and E2 and E3 are floated at the same potential. The center of the cell coincides with the PD laser irradiation spot. Each product ion peak ($m_2^+$) in a voltage-off PD spectrum splits into several components when high voltage is applied to the cell—the ones due to its formation from the precursor ion ($m_1^+$) inside (in-cell component, I) and outside (postcell component, P) the cell, and the consecutive components (C, $m_1^+ \rightarrow m_i^+ \rightarrow m_2^+$) with the first step occurring inside the cell and the second step outside. I and C are due to dissociation of $m_1^+$ within around 0.1 $\mu$s after photoexcitation, and P is due to dissociation occurring on the time scale of 0.2−5.0 $\mu$s.

**Detector Gain Calibration.** Voltage-on PD spectra for several peptide ions were measured at very low PD laser intensity such that each ion pulse in a single shot spectrum is due to one ion. Relative gain of MCP at each $m/z$ was determined by measuring the data system output per single ion pulse. Gain calibration curves for I and P components are drawn as a function of the fractional mass (product ion mass ÷ precursor ion mass) of product ions in Figure 2. The gain curve for PSD is the same as that for P. Gain for a C component is estimated by interpolation based on its relative position between the corresponding I and P components.

**Sample Preparation.** The peptide samples YYYYYY ($Y_6$) and $F_5$ with 90% purity were purchased from Peptron (Daejeon, Korea) and YPFVEPI with better than 95% purity from Sigma (St. Louis, MO). The matrices, 2,5-dihydroxybenzoic acid (DHB), sinapinic acid (SA), and α-cyano-4-hydroxycinnamic acid (CHCA), and other chemicals were purchased from Sigma. A matrix solution was prepared daily using acetonitrile and 0.1% trifluoroacetic acid and was mixed with a peptide solution. The final peptide concentrations prepared for PD experiments were 50 pmol/$\mu$L. One microliter of the solution was loaded on the sample plate.

**Principle of the Method.** The main assumption in this work is that RRKM is an adequate description for peptide ion dissociation. It will be shown later that PSD and time-resolved PD spectra obtained in this work are qualitatively compatible with the RRKM picture. It is widely accepted[20] that a MALDI

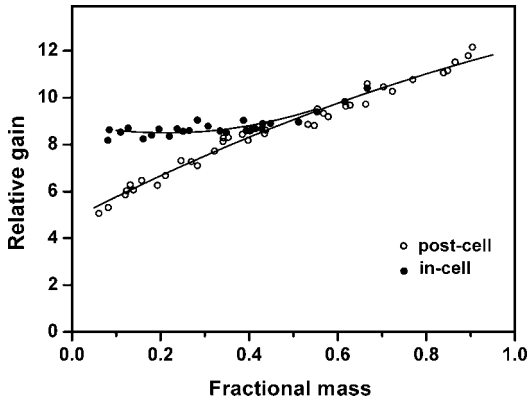


**Figure 2.** Relative gains of the MCP detector for post-cell (○) and in-cell (●) components drawn as a function of the fractional mass (product ion mass ÷ precursor ion mass). Several peptide ions were used in the measurement. −2.45 kV was applied to MCP.

plume is dense enough such that local thermal equilibrium is approached. Hence, we will make the second assumption that the internal degrees of freedom of a peptide ion are also in thermal equilibrium at a specified temperature $T$.

A systematic method to calculate the microcanonical rate constant $k(E)$ and the internal energy distribution for peptide ions at specified values of $E_0$, $\Delta S^{\ddagger}$, and $T$ was reported previously.[35−37] In the original report, six low frequency vibrations at the reactant equilibrium geometry were adjusted to get the vibrational frequency set at the transition state with specified $\Delta S^{\ddagger}$. This resulted in unphysical frequencies at the transition state when $\Delta S^{\ddagger}$ was large negative. Instead of six, thirty low frequency vibrations were adjusted in this work, even though $k(E)$ thus obtained was not significantly different from the one obtained by six frequency adjustment. When cleavages of more than one amide bond compete, the total rate constant is the sum of the individual rate constants. For the peptide ions dealt with in this work, product ions are formed via dissociation at various amide bonds along the b−y reaction paths. Under the assumption of the averaged treatment, $k(E)$ calculated for the cleavage of one amide bond was multiplied by the number of amide bonds to estimate the total dissociation rate constant, $k_t(E)$. $k_t(E)$ and $P_0(E)$ calculated for the peptide ion $[Y_6 + H]^+$ with $E_0 = 0.56$ eV, $\Delta S^{\ddagger} = -25.3$ eu (1 eu = 4.184 J K$^{-1}$ mol$^{-1}$), and $T = 400$ K are shown in Figure 3.

As precursor ions with the initial internal energy distribution $P_0(E)$ move along the ion-optical trajectory in the instrument, some of them will dissociate. Hence, the relative population ($P(E)$) of the surviving precursor ions with energy $E$ will decrease exponentially, $\exp(-k_t(E)t)$. Then, without PD laser irradiation, $P(E)$ at any time is given by the following relation.

$$P(E) = P_0(E) \exp(-k_t(E)t) \quad (1)$$

Arrival times of the precursor ion at various locations referred to two different time zeroes ($t_1$−$t_4$ referred to MALDI laser pulsing time in the absence of the cell voltage and $t_1{}^V$−$t_3{}^V$ referred to PD laser pulsing time in the presence of the cell voltage $V$) are marked in Figure 1. The photoexcitation time in the presence of the cell voltage is slightly different from the one in its absence ($t_2$). The former is taken as the time zero in $t_i{}^V$ time scale. $P(E)$'s at the times $t_1$−$t_4$ are marked as $P_1$, $P_2$, etc. in Figure 3b. The area under each curve will be called $A_0$ (=1), $A_1$, $A_2$, etc. It is to be mentioned that $P_i(E)$'s are unnormalized distribution functions and $A_i$'s represent relative

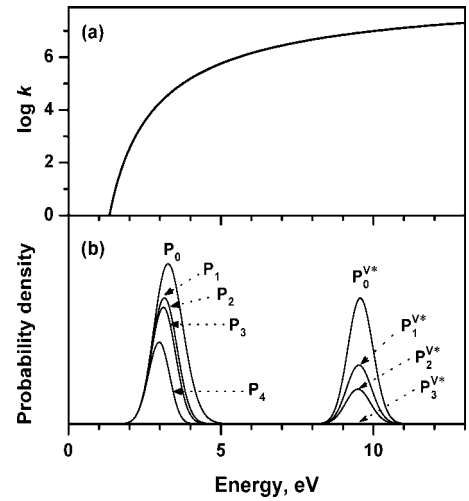


**Figure 3.** (a) $k_t(E)$ and (b) $P_0(E)$ for $[Y_6 + H]^+$ calculated with $E_0 = 0.56$ eV, $\Delta S^{\ddagger} = -25.3$ eu, and $T = 400$ K. $P_i(E)$'s are distributions at various locations marked in Figure 1. $P_i{}^{V*}(E)$ are distributions after absorption of one 193 nm photon, calculated for voltage-on (3 kV) PD at various locations.

intensities of a precursor ion beam at various positions. Shifting $P(E)$ at the laser irradiation position along the abscissa by the photon energy results in the $P(E)$ curve upon photoexcitation, or $P_0{}^{V*}(E)$, with the area $A_0{}^{V*}$. The internal energy distributions for photoexcited precursor ions at other locations can be calculated using $t_i{}^V$ time scale as follows.

$$P_i^{V*}(E) = P_0^{V*}(E) \exp(-k_t(E)t_i^V) \quad (2)$$

The area under each curve will be called $A_i{}^{V*}$.

In PSD, the measured intensity of the precursor ion will correspond to $A_4$. As mentioned already, PSD product ions generated in front of the first time focus are eliminated by the deflection system. Because the measured PSD occurs during $t_1$−$t_3$ and the corresponding precursor ion intensities are $A_1$ and $A_3$, respectively, one might take $A_1$−$A_3$ as the total PSD intensity. A problem is that both the precursor and product ions further dissociate inside the reflectron. Rate constant calculations taking into account the fact that some energy is lost in dissociation show that product ions, on the average, dissociate less efficiently in this region than the precursor ion. This leads to the following inequalities for the measured [total PSD]/[precursor] ratio (YPSD).

$$(A_1 - A_3)/A_3 \le \text{YPSD} \le (A_1 - A_3)/A_4 \quad (3)$$

Instead of the total PD yield, we used the ratio of total product ion yields formed outside and inside the cell, $\Sigma[P]/\Sigma[I + C] =$ CPD, in the kinetic analysis. Its theoretical value at the reflectron entrance is $(A_2{}^{V*} - A_3{}^{V*})/(A_0{}^{V*} - A_1{}^{V*})$. We estimated ±30% error for CPD from this theoretical value and used the following inequalities.

$$0.7\ \text{CPD} \le (A_2^{V*} - A_3^{V*})/(A_0^{V*} - A_1^{V*}) \le 1.3\ \text{CPD} \quad (4)$$

## Results and Discussion

PSD spectra of $[Y_6 + H]^+$ generated by MALDI using DHB, SA, and CHCA as matrices are shown in Figure 4. Regardless

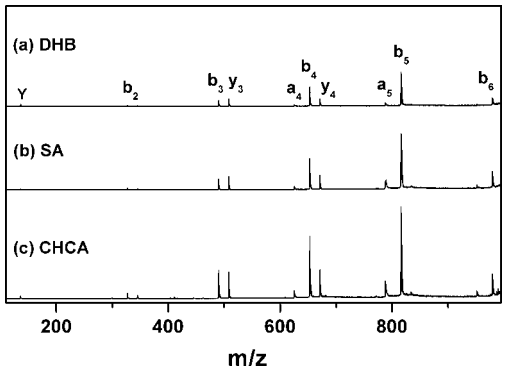


**Figure 4.** PSD spectra of $[Y_6 + H]^+$ generated by MALDI using (a) DHB, (b) SA, and (c) CHCA as matrices. Product ion peak heights are normalized to that of the precursor ion in each spectrum. Total PSD yield is in the order DHB < SA < CHCA.

of the matrices used in MALDI, $b_n$ ($n = 2-6$) and $y_n$ ($n = 3$, 4) were the major product ions. $a_n$ ($n = 4$, 5) also appeared, probably via loss of CO from $b_n$.[10] This suggests that the averaged single channel treatment adopted in this work can be a reasonable approximation. The PSD intensities were in the order DHB < SA < CHCA, with the calibrated YPSD values being 0.16, 0.46, and 0.72, respectively, for MALDI with these matrices. This trend is in agreement with the general perception[24] that DHB, SA, and CHCA are "cold", "intermediate", and "hot" matrices, respectively, in peptide MALDI. The trends observed for PSD of $[F_5 + H]^+$ and $[YPFVEPI + H]^+$ were similar as summarized in Table 1.

Voltage-on 193 and 266 nm PD spectra of $[Y_6 + H]^+$ formed by MALDI with the same matrices are shown in Figure 5. Splitting of each product ion peak into the in-cell (I), post-cell (P), and consecutive (C) components due to the cell voltage are marked in the figure. In PD also, $b_n$ ($n = 2$, 3) and $y_n$ ($n = 2$) are the major product ions, with some contribution from $a_2$ and the immonium ion Y. Compared to the PSD spectra, the sizes of $b_n$ and $y_n$ ions are smaller (smaller $n$) in the PD spectra. According to our previous time-resolved PD study[32] on some peptide ions without a basic amino acid residue, large internal energy supplied by photoabsorption induces further dissociation of a first generation product ion, b type ions to smaller b and y type ions to smaller y. This must be responsible for the consecutive components in Figure 5. Hence, the sum of the intensities for I and C components represents the total dissociation yield inside the cell and that of the P components represents the dissociation yield outside the cell. Compared to the post-cell component, combined intensity of the in-cell and consecutive components for each product ion peak is more prominent in 193 nm PD than in 266 nm PD, in qualitative agreement with the RRKM picture. A similar trend was observed in PD of $[F_5 + H]^+$ (not shown). Such an orderly trend for each product ion peak was not seen in PD of $[YPFVEPI + H]^+$ due to complications arising from the participation of consecutive reactions. Regardless, the trend held for the sums over the product ions, as can be seen from CPD values listed in Table

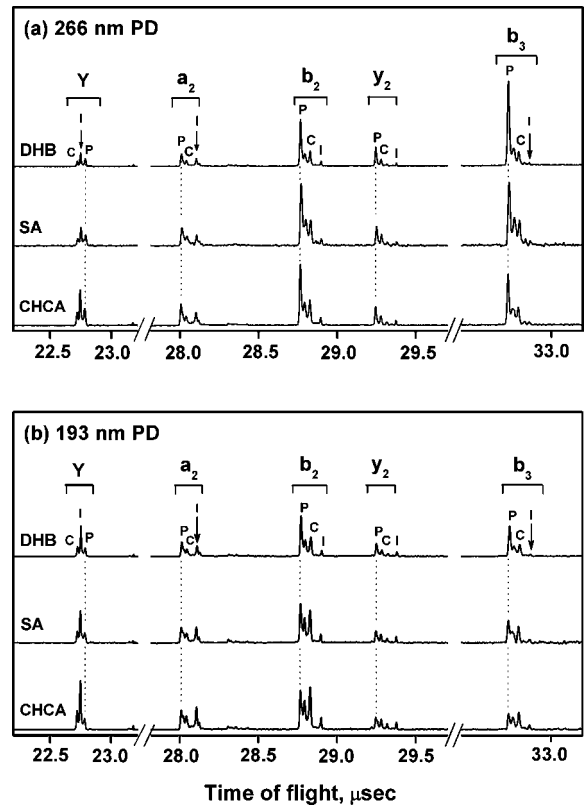


**Figure 5.** Product ion peak splitting patterns in the voltage-on (a) 266 and (b) 193 nm PD of $[Y_6 + H]^+$. Three kilovolts was applied to the cell. I and C are due to dissociation of $[Y_6 + H]^+$ inside the cell within 93 ns after photoexcitation, and P components are formed outside the cell during 0.16−5.0 $\mu$s.

1. Also to be noted from the data in Table 1 is the order DHB > SA > CHCA for CPD determined by 266 and 193 nm PD. That is, photodissociation of peptide ions formed by DHB-MALDI (these ions have lower internal energy than those by CHCA-MALDI, as observed in PSD) occurs more slowly than those formed by CHCA-MALDI. This is also in agreement with the RRKM picture.

With three adjustable parameters ($E_0$, $\Delta S^{\ddagger}$, and $T$) it was a formidable task to determine a parameter set(s) that is compatible with the experimental YPSD and CPD data, especially because we did not have any idea on their magnitudes. Hence, we attempted grid search. That is, $k_t(E)$ and $P_0(E)$ were calculated with 2 600 000 different sets of ($E_0$, $\Delta S^{\ddagger}$, $T$), $E_0$ at 0.005 eV interval, $\Delta S^{\ddagger}$ at 0.25 eu interval, and $T$ at 20 K interval, from which $A_i$ and $A_i^{V*}$ were evaluated. From these, the sets simultaneously satisfying eq 3 for PSD and eq 4 for 193 and 266 nm PD were selected. $E_0$, $\Delta S^{\ddagger}$, and $T$ of the sets satisfying these equations for $[Y_6 + H]^+$ formed by CHCA-MALDI are shown as blue spheres in Figure 6. It is obvious that $E_0$, $\Delta S^{\ddagger}$, and $T$ cannot be narrowly determined in this case. The sets determined under the SA- and DHB-MALDI conditions are also shown in the figure. Accuracy for parameter determination is

**TABLE 1: Experimental YPSD and CPD data for $[Y_6 + H]^+$, $[F_5 + H]^+$, and $[YPFVEPI + H]^+$ Peptide Ions Generated by MALDI with DHB, SA, and CHCA as Matrices**

| | | $[Y_6 + H]^+$ | | | $[F_5 + H]^+$ | | | $[YPFVEPI + H]^+$ | | |
|---|---|---|---|---|---|---|---|---|---|---|
| | | DHB | SA | CHCA | DHB | SA | CHCA | DHB | SA | CHCA |
| YPSD | | 0.160 | 0.459 | 0.722 | 0.114 | 0.298 | 0.497 | 0.037 | | 0.458 |
| CPD | 193 nm | 0.717 | 0.508 | 0.282 | 0.414 | 0.219 | 0.156 | 1.980 | | 1.276 |
| | 266 nm | 1.672 | 0.938 | 0.829 | 0.999 | 0.642 | 0.390 | 4.083 | | 2.424 |

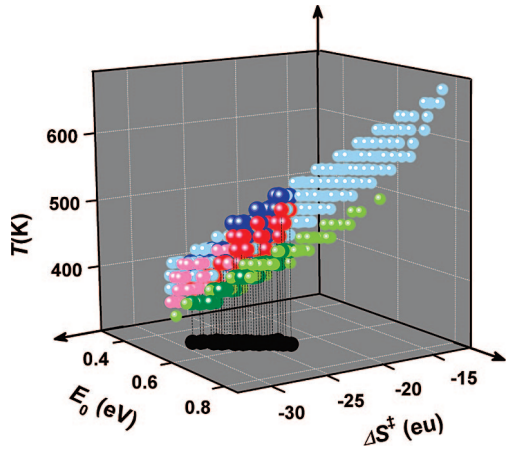


**Figure 6.** ($E_0$, $\Delta S^{\ddagger}$, $T$) sets simultaneously satisfying eq 3 for PSD and eq 4 for 193 and 266 nm PD of $[Y_6 + H]^+$ generated by MALDI using DHB (green), SA (red), and CHCA (blue) as matrices. For each set, the subset which shares common $E_0$ and $\Delta S^{\ddagger}$ values in the three sets, but different $T$, is represented by spheres with deeper color. Corresponding ($E_0$, $\Delta S^{\ddagger}$) region is shown as a shadow at the bottom plane.

better in the latter cases. Accuracy would further improve if the sets obtained from the three cases are considered together by taking into account the fact that $E_0$ and $\Delta S^{\ddagger}$ of the reactions are the same regardless of the matrices used, whereas the temperatures are different. Graphically, correct sets can be found by projecting each sphere to the bottom plane ($E_0-\Delta S^{\ddagger}$) and selecting those for which the projections of the three different matrix data sets overlap. The spheres meeting this criterion are marked in deep blue, red, and green colors in Figure 6. $E_0$, $\Delta S^{\ddagger}$, and $T$ determined from the data set of deep colored spheres are listed in Table 2. The analysis was done for $[F_5 + H]^+$ and $[YPFVEPI + H]^+$ also. The results are also listed in Table 2. It is to be noted that the parameters determined for three different peptide ions (none of these contains a basic amino acid residue) are similar.

According to previous quantum chemical calculations,[11,28] $E_0$ for the dissociation of $[G_3 + H]^+$ to $b_2$ product ion was 1.14 eV, much larger than around 0.6 eV found in this work. $\Delta S^{\ddagger}$ estimated for the reported transition state was −2.65 eu, also much larger than around −24 eu found in this work. We do not have an explanation for such large discrepancies. A possibility is that intramolecular interaction in the transition structure gets more important as peptide gets larger, resulting in smaller $E_0$ and $\Delta S^{\ddagger}$. In our previous time-resolved PD study,[8] $E_0$ and $\Delta S^{\ddagger}$ close to the theoretical results were used to qualitatively explain the experimental trends. Using the same $E_0$ and $\Delta S^{\ddagger}$ values as used in the previous work, we attempted to estimate how far off the results were from the present experimental data. We chose temperatures such that the calculated $(A_1-A_3)/A_3$ and $(A_1-A_3)/A_4$ satisfied eq 3. Then, it was found that the calculated $({A_2}^{V*} - {A_3}^{V*})/({A_0}^{V*} - {A_1}^{V*})$ was smaller than experimental CPD by more than an order of magnitude. That is, $E_0$ and $\Delta S^{\ddagger}$ values used in the previous qualitative work failed to quantitatively explain the present experimental results.

Futrell and co-workers[13] measured time evolution of product ion signals in SID of some peptide ions and derived $E_0$ and $\Delta S^{\ddagger}$ for the formation of each product ion. As mentioned in the Introduction, insufficient knowledge about energy transfer in SID is a problem in such an effort. Another problem is that an activated peptide ion undergoes complicated competing and consecutive reactions, as seen in this work and in our previous work.[8] It is our opinion that $E_0$ and $\Delta S^{\ddagger}$ for a particular reaction path cannot be correctly determined without accounting for the participation of consecutive reactions.

The internal temperature of the peptide ions formed by MALDI in this work was in the order DHB (400 K) < SA (440 K) < CHCA (460 K), in agreement with the general qualitative perception on peptide MALDI. This is in contrast with the order DHB > SA > CHCA for matrix plume temperature observed in laser-induced desorption of molecular ions embedded in a matrix—MALD of preformed ions.[22] Reversal in the order means that the internal temperature of a peptide ion is different from the matrix plume temperature. There is a general consensus[20] that proton transfer reactions occurring in the plume are mainly responsible for the formation of peptide ions, or protonated peptide to be more rigorous. Then, the internal temperature of a peptide ion would be affected not only by the plume temperature but also by $\Delta H$ in proton transfer reactions. Assuming that protonated matrix is the acid in the gas phase acid−base (proton transfer) reaction, use of a matrix with larger proton affinity (PA) would form a peptide ion with lower internal temperature. A problem in this regard is the fact that PA values for common matrices are not well established yet. According to a compilation of matrix PA data reported in a recent review article by Knochenmuss,[20] PAs are in the range 766−933 for CHCA, 876−895 for SA, and 850−856 kJ mol$^{-1}$ for DHB. Even though the data for CHCA are widely scattered, the data for SA are consistently larger than those for DHB. However, a larger PA for SA is not compatible with higher $T$ of peptide ions formed with SA than those with DHB. It is to be emphasized that all the spectral patterns obtained in this work suggest higher $T$ with SA than with DHB. This is probably correct even if our analysis might possibly have been erroneous. Hence, we are forced to conclude that the matrix PA data hitherto determined are unreliable or that protonated matrices are not the major acids in proton transfer reactions or that the internal energy of a peptide ion is not determined by the proton transfer reaction. At the moment, we do not have any explanation for the order DHB < SA < CHCA in the peptide ion temperature.

## Conclusion

There have been many experimental and computational attempts[21−24,38−40] to measure or estimate the temperatures of matrix−analyte substrate after MALDI laser irradiation, of matrix plume, and of ions formed by MALDI. There also have been quantum chemical and experimental efforts to determine

**TABLE 2: Average Temperature (K) of Peptide Ions Generated by MALDI with DHB, SA, and CHCA as Matrices and $E_0$ (eV) and $\Delta S^{\ddagger}$ (eu) for Their Dissociation**

| | | | average temperature | | |
|---|---|---|---|---|---|
| | $E_0$ | $\Delta S^{\ddagger}$ | DHB | SA | CHCA |
| $[Y_6 + H]^+$ | 0.56 ± 0.03 | −25.3 ± 1.4 | 400 ± 21 | 440 ± 29 | 460 ± 31 |
| $[F_5 + H]^+$ | 0.57 ± 0.02 | −24.1 ± 0.9 | 404 ± 15 | 437 ± 13 | 470 ± 25 |
| $[YPFVEPI + H]^+$ | 0.65 ± 0.03 | −24.0 ± 1.0 | 427 ± 16 | | 507 ± 16 |

$E_0$ and $\Delta S^{\ddagger}$ for dissociation of peptide ions along b−y reaction paths. Application of the kinetic method devised in this work for simultaneous determination of $E_0$, $\Delta S^{\ddagger}$, and $T$ to some peptide ions without a basic residue found somewhat low magnitudes for these parameters. Reliability of the present technique is likely to depend on the validity of the two major assumptions made (thermal equilibrium for peptide ions formed by MALDI and their statistical dissociation), which need further test.

Capability to measure the effective internal temperature of a molecular ion developed in this work will be useful in the investigation of the fundamentals of ion formation in MALDI. Particularly useful will be the measurement of the effective internal temperature in MALDI with matrices and peptides with widely different proton affinities.

In tandem mass spectrometry of peptide ions, various residue-specific spectral correlations have been observed.[8,10,41] An example is the changeover[10] from the rearrangements (b−y) to homolytic cleavage channels for peptide ions with an arginine residue as the energy regime changes from low to high. Acquisition of experimental data for $E_0$ and $\Delta S^{\ddagger}$ may be useful to find explanations for such outstanding problems.

**Acknowledgment.** This work was financially supported by Korea Research Foundation, Republic of Korea and by the Biosignal Analysis Technology Innovation program (M10645010-002-06N4501-00210) of the Ministry of Science and Technology, Republic of Korea. S.H.Y. thanks the Ministry of Education, Republic of Korea, for Brain Korea 21 Fellowship.

## References and Notes

(1) Kinter, M.; Sherman, N. E. *Protein Sequencing and Identification Using Tandem Mass Spectrometry*; John Wiley: New York, 2000; pp 64−116, 238−268.
(2) Hernandez, P.; Müller, M.; Appel, R. D. *Mass Spectrom. Rev.* **2006**, *25*, 235.
(3) Holbrook, K. A.; Pilling, M. J.; Robinson, S. H. *Unimolecular Reactions*; Wiley: Chichester, U.K., 1996; pp 39−78.
(4) Liftshitz, C. *Adv. Mass Spectrom.* **1989**, *11A*, 713.
(5) Baer, T.; Mayer, P. M. *J. Am. Soc. Mass Spectrom.* **19997**, *8*, 103.
(6) Park, S. T.; Kim, S. K.; Kim, M. S. *Nature* **2002**, *415*, 306.
(7) Choi, K. M.; Yoon, S. H.; Sun, M.; Oh, J. Y.; Moon, J. H.; Kim, M. S. *J. Am. Soc. Mass Spectrom.* **2006**, *17*, 1643.
(8) Yoon, S. H.; Chung, Y. J.; Kim, M. S. *J. Am. Soc. Mass Spectrom.* **2008**, *19*, 645.
(9) Roepstorff, P.; Fohlman, J. *Biomed. Mass Spectrom.* **1984**, *11*, 601.
(10) Johnson, R. S.; Martin, S. A.; Biemann, K. *Int. J. Mass Spectrom. Ion Processes* **1988**, *86*, 137.
(11) Paizs, B.; Suhai, S. *Rapid Commun. Mass Spectrom.* **2002**, *16*, 375.
(12) El Aribi, H.; Rodriquez, C. F.; Almeida, D. R. P.; Ling, Y.; Mak, W. W. N.; Hopkinson, A. C.; Siu, K. W. M. *J. Am. Soc. Mass Spectrom.* **2003**, *125*, 9229.
(13) Laskin, J.; Bailey, T. H.; Furtrell, J. H. *Int. J. Mass Spectrom.* **2004**, *234*, 89.
(14) Mabud, M. D. A.; Dekrey, M. J.; Cooks, R. G. *Int. J. Mass Spectrom. Ion Processes* **1985**, *67*, 285.
(15) Laskin, J.; Furtrell, J. H. *Mass Spectrom. Rev.* **2003**, *22*, 158.
(16) Hillencamp, F.; Karas, M.; Beavis, R. C.; Chait, B. T. *Anal. Chem.* **1991**, *63*, 1193A.
(17) Dreisewerd, K. *Chem. Rev.* **2003**, *103*, 395.
(18) Karas, M.; Krüger, R. *Chem. Rev.* **2003**, *103*, 427.
(19) Knochenmuss, R.; Zenobi, R. *Chem. Rev.* **2003**, *103*, 441.
(20) Knochenmuss, R. *Analyst* **2006**, *131*, 966.
(21) Mowry, C. D.; Johnston, M. V. *J. Phys. Chem.* **1994**, *98*, 1904.
(22) Luo, G.; Marginean, I.; Vertes, A. *Anal. Chem.* **2002**, *74*, 6185.
(23) Bencsura, A.; Navale, V.; Sadeghi, M.; Vertes, A. *Rapid Commun. Mass Spectrom.* **1997**, *11*, 679.
(24) Gabelica, V.; Schulz, E.; Karas, M. *J. Mass Spectrom.* **2004**, *39*, 579.
(25) Schulz, E.; Karas, M.; Rosu, F.; Gabelica, V. *J. Am. Soc. Mass Spectrom.* **2006**, *17*, 1005.
(26) Knochenmuss, R.; Stortelder, A.; Breuker, K.; Zenobi, R. *J. Mass Spectrom.* **2000**, *35*, 1237.
(27) Kinsel, G. R.; Preston, L. M.; Russell, D. H. *Biol. Mass Spectrom.* **1994**, *23*, 205.
(28) Paizs, B.; Suhai, S. *Mass Spectrom. Rev.* **2005**, *24*, 508.
(29) Paizs, B.; Suhai, S. *J. Am. Soc. Mass Spectrom.* **2004**, *15*, 103.
(30) Paizs, B.; Schnölzer, M.; Warnken, U.; Suhai, S.; Harrison, A. G. *Phys. Chem. Chem. Phys.* **2004**, *6*, 2691.
(31) Spengler, B.; Lützenkirchen, F.; Kafumann, R. *Org. Mass Spectrom.* **1993**, *28*, 1482.
(32) Yoon, S. H.; Kim, M. S. *J. Am. Soc. Mass Spectrom.* **2007**, *18*, 1729.
(33) Yoon, S. H.; Moon, J. H.; Choi, K. M.; Kim, M. S. *Rapid Commun. Mass Spectrom.* **2006**, *20*, 2201.
(34) Moon, J. H.; Yoon, S. H.; Kim, M. S. *Bull. Korean Chem. Soc.* **2005**, *26*, 763.
(35) Moon, J. H.; Oh, J. Y.; Kim, M. S. *J. Am. Soc. Mass Spectrom.* **2006**, *17*, 1749.
(36) Sun, M.; Moon, J. H.; Kim, M. S. *J. Phys. Chem. B* **2007**, *111*, 2747.
(37) Moon, J. H.; Sun, M.; Kim, M. S. *J. Am. Soc. Mass Spectrom.* **2007**, *18*, 1063.
(38) Zhigilei, L. V.; Leveugle, E. *Chem. Rev.* **2003**, *103*, 321.
(39) Knochenmuss, R.; Zhigilei, L. V. *J. Phys. Chem. B* **2005**, *109*, 22947.
(40) Greisch, J. F.; Gabelica, V.; Remacle, F.; Pauw, E. *Rapid Commun. Mass Spectrom.* **2003**, *17*, 1847.
(41) Wysocki, V. H.; Tsaprailis, G.; Smith, L. L.; Breci, L. A. *J. Mass Spectrom.* **2000**, *35*, 1399.

JP810077E